A Fabrication Route for the Production of Co-Planar, Diamond Insulated, Boron Doped Diamond Macro and Microelectrodes of any Geometry.

ARTICLE *in* ANALYTICAL CHEMISTRY · MAY 2014

Impact Factor: 5.64 · DOI: 10.1021/ac501092y · Source: PubMed

8 AUTHORS, INCLUDING:

Eleni Bitziou
The University of Warwick
19 PUBLICATIONS **246** CITATIONS
SEE PROFILE

Tania Louise Read
The University of Warwick
7 PUBLICATIONS **31** CITATIONS
SEE PROFILE

Mark Edward Newton
The University of Warwick
105 PUBLICATIONS **1,784** CITATIONS
SEE PROFILE

Julie V Macpherson
The University of Warwick
175 PUBLICATIONS **5,629** CITATIONS
SEE PROFILE

analytical chemistry

Technical Note

pubs.acs.org/ac

Fabrication Route for the Production of Coplanar, Diamond Insulated, Boron Doped Diamond Macro- and Microelectrodes of any Geometry

Maxim B. Joseph,[†] Eleni Bitziou,[†] Tania L. Read,[†] Lingcong Meng,[†] Nicola L. Palmer,[§] Tim P. Mollart,[§] Mark E. Newton,[‡] and Julie V. Macpherson*,[†]

[†]Department of Chemistry and [‡]Department of Physics, University of Warwick, Coventry, West Midlands CV4 7AL, United Kingdom

[§]Element Six Ltd., Element Six Global Innovations Centre, Harwell Campus, Didcot, Oxfordshire OX11 0QR, United Kingdom

Supporting Information

ABSTRACT: Highly doped, boron doped diamond (BDD) is an electrode material with great potential, but the fabrication of suitable electrodes in a variety of different geometries both at the macro- and microscale, with an insulating material that does not compromise the material properties of the BDD, presents technical challenges. In this Technical Note, a novel solution to this problem is presented, resulting in the fabrication of coplanar macro- and microscale BDD electrodes, insulated by insulating diamond, at the single and multiple, individually addressable level. Using a laser micromachining approach, the required electrode(s) geometry is machined into an insulating diamond substrate, followed by overgrowth of high quality polycrystalline BDD (pBDD) and polishing to reveal approximately nanometer roughness, coplanar all-diamond structures. Electrical contacting is possible using both top and bottom contacts, where the latter are defined using the laser to produce non-diamond-carbon (NDC) in the vicinity of the back side of the BDD. We present the fabrication of individually addressable ring, band, and disk electrodes with minimum, reproducible controlled dimensions of 50 μm (limited only by the laser system employed). The pBDD grown into the insulating diamond recesses is shown to be free from NDC and possesses excellent electrochemical properties, in terms of extended solvent windows, electrochemical reversibility, and capacitance.

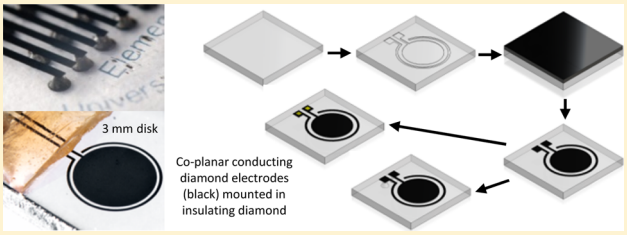

Boron doped diamond (BDD) is an interesting electrode material due to its ultrawide solvent window in aqueous media, low capacitive currents, and high resistance to fouling and corrosion.[1] BDD for electrochemical applications is typically polycrystalline (pBDD), synthesized in either micro- or nanocrystalline thin film form on a conducting or insulating substrate. If the pBDD is grown thick enough, the material can be removed from the growth substrate and is freestanding. Note, typically, the thicker the material, the larger the crystallite size. Non-diamond-carbon (NDC) content can be high in nanocrystalline BDD and, unless growth is very carefully controlled, is also prevalent in microcrystalline BDD.[2]

For electrochemical studies, a cell of defined geometry is typically placed, or clamped, over the electrode to create a defined geometric area.[3] Electrical contact is either made to the base (if the substrate is conducting) or through a top contact (if the substrate is insulating). For freestanding pBDD, the material can also be machined into a defined structure, e.g., a cylinder, cuboid, etc., electrically back-contacted, and then sealed in glass[4] or an insulating polymer, such as PTFE,[5] epoxy,[3b,6] or PEEK[7] to produce electrode formats more akin to commercially available, conventional electrode materials such as Pt, Au, and glassy carbon. Disk electrodes with diameters in the range of tens of micrometers[8] to several millimeters[2,9] have been fabricated this way. pBDD microelectrodes have also been produced by growing thin films of pBDD onto sharpened W wires and sealing with epoxy and glass.[10] However, in all cases, the mechanical and chemical stability of the material used to insulate is always inferior to that of the pBDD, limiting potential applications.

Moving to an all-diamond format offers several advantages, including: (i) formation of a robust seal between the pBDD electrode and insulating diamond; (ii) resistance to chemical and thermal stress and abrasive wear; and (iii) longevity in extreme environments. There have so far been limited attempts to produce all-diamond electrodes. Using freestanding pBDD, laser ablation was used to define pillar structures in pBDD. Subsequent overgrowth with insulating diamond and polishing revealed an array of coplanar pBDD microdisk electrodes, 10–50 μm in diameter. However, this approach meant that the array was not individually addressable and insulating diamond growth needed to be carefully controlled to ensure no defects,

Received: March 26, 2014
Accepted: May 9, 2014

   dx.doi.org/10.1021/ac501092y | *Anal. Chem.* XXXX, XXX, XXX–XXX

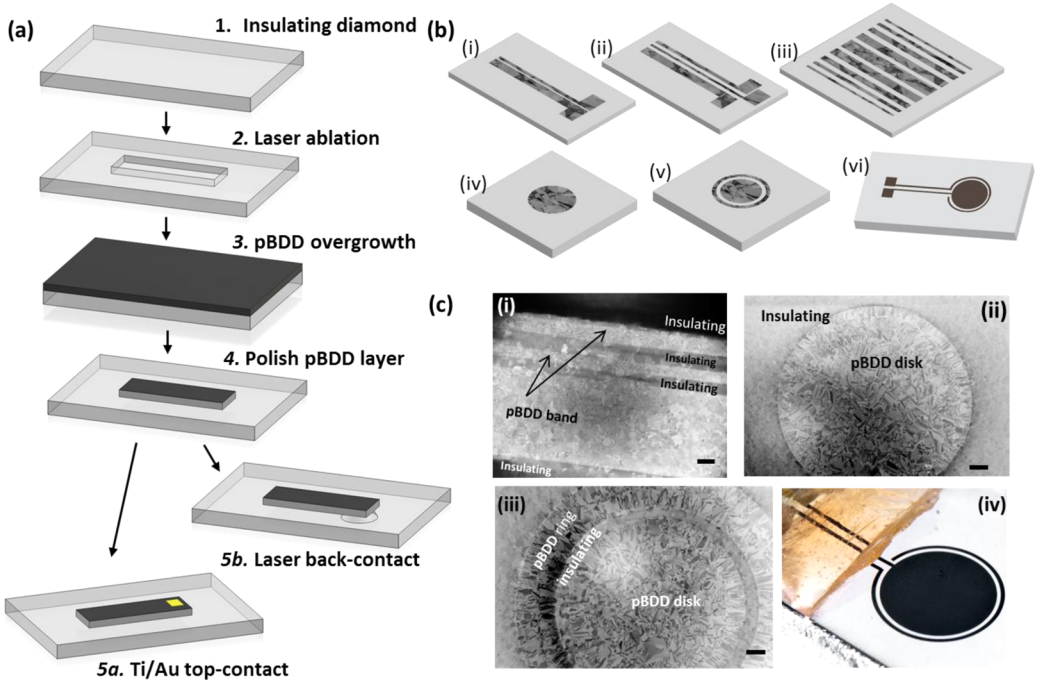

Figure 1. (a) Schematic describing the step-by-step fabrication of the all-diamond electrodes. (b) 3D schematics of different all-diamond pBDD electrodes fabricated using the process described in (a). (i) dual band; (ii) triple band; (iii) multiple bands; (iv) disk; (v, vi) ring disk. (i, ii, and vi) contain contact pads for top electrical contacts. (c, i–iii) FE-SEM images of all-diamond devices: (i) triple band (in-lens); (ii) macrodisk (secondary electron, SE); and (iii) ring disk (SE) (dimensions in text). (c, iv) Optical photograph (image Copyright 2014 Jonathan C. Newland) of a top contacted ring disk (disk is 3 mm diameter) all diamond electrode. All scale bars are 100 μm. Note the contrast has been reversed in (ii, iii) in order to emphasize the BDD electrodes.

pinholes, or cracks in the overgrowth layer.[11] A three layer diamond growth process was also described, where a microlayer of pBDD was sandwiched between two intrinsic diamond layers. A macrohole cut through the structure resulted in the formation of an all-diamond ring electrode, suitable for use in flow studies.[12] Finally, nanocrystalline BDD, patterned to isolate insulating diamond overgrowth from defined regions, resulted in a nonaddressable recessed BDD UME electrode array.[13]

In this Technical Note, we describe for the first time an alternative fabrication route resulting in the production of coplanar all-diamond electrodes, of any geometry, both at the macro- and microscale. Single or multiple, individually addressed electrodes can be produced on one device. We highlight the method by demonstrating the fabrication and characterization of individually addressable disks, bands, and ring disk geometries, suitable for a wide range of electrochemical applications. Our novel all-diamond devices are fully characterized using Raman spectroscopy, electron microscopy, conductivity measurements, and electrochemistry.

EXPERIMENTAL SECTION

Reagents and Solutions. All solutions were prepared with Milli-Q water (Millipore Corp., UK) with a resistivity of 18.2 Ω at 25 °C. To characterize the pBDD electrodes, solutions of 0.1 M KNO_3 (Sigma-Aldrich, UK) were used for solvent windows and capacitance experiments. For cyclic voltammetry (CV) measurements, solutions contained 1 mM hexaammineruthenium(III) chloride ($Ru(NH_3)_6^{3+}$: Strem Chemicals, Newbury Port, USA) in 0.1 M KNO_3.

Materials. Microwave chemical vapor deposition (MW-CVD) polycrystalline insulating synthetic diamond was fabricated by Element Six (Harwell, Oxford, UK) in disk form (25 mm diameter). Typically, the substrates were 1 mm in thickness, mechanically lapped (polished) to a surface roughness of <2 nm, and then subject to laser micromachining using a high power laser micromachiner (E-355H-3-ATHI-O, Oxford Lasers, UK). The resulting structures were acid cleaned in hot (~200 °C) concentrated sulfuric acid saturated with KNO_3, to remove any NDC produced during lasering.[14] pBDD overgrowths were carried out using MW-CVD on the processed substrates. The approximate growth conditions used to prepare the appropriately doped "metal-like" pBDD films have been described previously.[15] Electrical top contacts to pBDD contact pads on the all-diamond electrodes were made by sputtering a Ti/Au (10 nm/300 nm) layer (Moorfields sputter system, UK) through a Kapton tape (DuPont, UK) mask and annealing at 400 °C for 5 h to produce an ohmic contact.[16] NDC (graphitized) contacts were made using the laser micromachiner (*vide supra*).

Electrical conductivity measurements were carried out on 1 × 1 × 10 mm pBDD bars (Diafilm Electroanalysis grade, of a similar quality to the overgrowth pBDD-Element Six)[2] on which four collinear contacts had been placed, either by graphitization (NDC) and AgDAG (Silver conductive paint, RS, UK) or by Au/Ti sputtering. Material characterization of the wafers was carried out using optical microscopy (BH-2, Olympus, UK), white light interferometry (Contour GT-K, Bruker, UK), field emission scanning electron microscopy (FE-SEM: Supra 55 VP, Zeiss), atomic force microscopy (AFM: Nano Enviroscope with Nanoscope IV controller, Bruker, UK), and Micro-Raman spectroscopy (Renishaw inVia Raman, Ar^+ laser at 514.5 nm excitation) using a 50× objective lens and a spot size of ~5 μm.

dx.doi.org/10.1021/ac501092y | *Anal. Chem.* XXXX, XXX, XXX–XXX

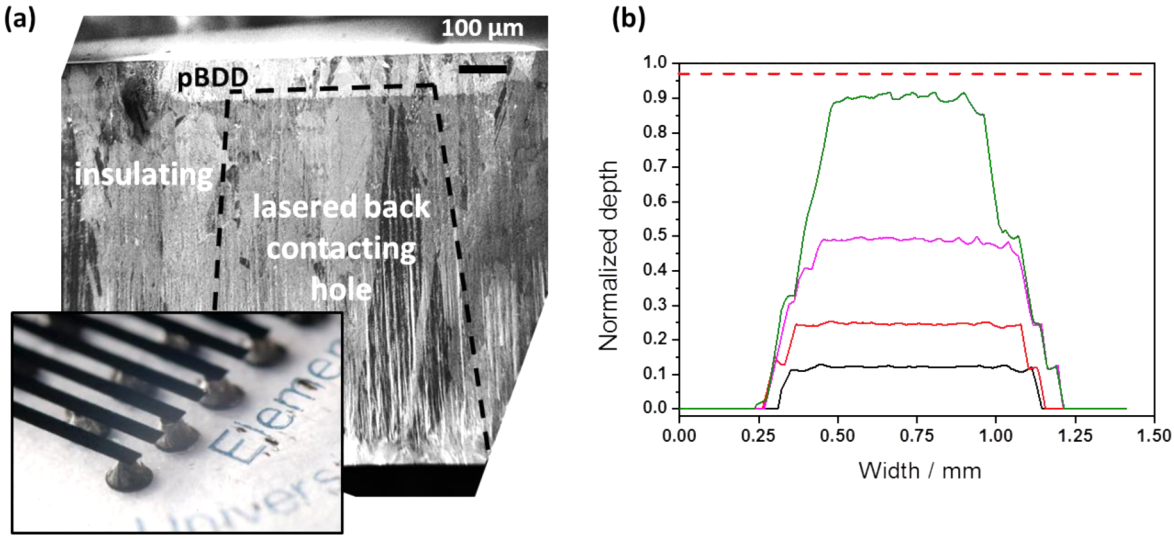

Figure 2. Back contacting the all-diamond electrodes: (a) In-lens FE-SEM image of a cross-sectioned macroelectrode disk structure. The pBDD is clearly evident as a region of lighter contrast at the top of the image. The internal surface of the electrode is contacted by laser micromachining a hole through the insulating diamond to the pBDD layer. Inset shows a photograph (image Copyright 2014 Jonathan C. Newland) looking through the transparent top surface of a multiple band electrode (at least seven black, boron doped, electrodes are visible). The lasered back contacts are visible as black cones. The bands are each 180 μm wide. (b) White light interferometry cross-sectional depth profiles taken at various stages during the laser micromachining process, demonstrating a high level of depth control. The y axis has been normalized with respect to the thickness of the diamond wafer (1 mm); the red dotted line indicates the front electrode face of the diamond.

Electrochemical Measurements. Electrochemical characterization of the all-diamond electrodes was performed in a standard three-electrode configuration using a Pt counter electrode and a reference electrode (saturated calomel electrode, SCE) for solvent window, capacitance, and redox electrochemical analysis. CV was carried out using a potentiostat (CHI740a, CH Instruments Inc., USA). The back contacted BDD electrodes were typically mounted into the lid of a polypropylene Falcon tube (Fisher Scientific, UK) using silicone sealant 786 (Dow Corning, UK) or cast in epoxy (RX771C/NC, Robnor, UK) such that the electrode bearing face was exposed to solution. For the top-contacted electrodes, the accessible electrode area was defined by epoxy glue or kapton tape. Current−voltage (resistance) curves were measured in air using a Keithley current source (Model 6220, Keithley).

Theoretical Modeling. A COMSOL (COMSOL multiphysics, COMSOL, SWE) model was employed to simulate the electrochemical CV behavior of the various electrode geometries fabricated as described in full in the Supporting Information, Section 1.

RESULTS AND DISCUSSION

All-Diamond Electrode Fabrication. The fabrication process employed to produce the all-diamond electrodes is shown schematically in Figure 1a. The starting substrate, insulating polycrystalline diamond, was laser micromachined using a high power laser micromachiner to produce recessed structures "trenches" where the base geometry reflects the resulting electrode geometry. pBDD was overgrown into the lasered trenches, and a coplanar structure was revealed through multidirectional polishing of the overgrown surface using a resin-bonded scaife embedded with diamond microparticles, 2−20 μm in size. Using this process, all-diamond macro- and microelectrode structures such as disks (cylindrical machined holes), bands (trenches), and ring electrodes (circular trenches), shown schematically in Figure 1b, were produced. Typical trench depths, i.e., initial electrode depth, varied from ca. 50 to 100 μm, although after overgrowth and polishing the resulting pBDD electrode depth was reduced.

The minimum feature size is theoretically defined by the minimum laser spot diameter, which for this system is ∼6 μm.[17] However, the entry hole for the laser spot is ∼20−30 μm in diameter as laser fluence (uniformity of energy density across the beam diameter) and the ablation threshold of the material are critical. The heterogeneous nature of polycrystalline diamond also means the laser ablation efficiency will vary between grains. We found that the minimum repeatable feature size on polycrystalline diamond was limited to ca. 50 μm × 50 μm with the laser system employed. Furthermore, as CVD diamond growth is dominated by surface kinetics,[18] the bottom of narrow and deep channels, where transport of growth species is lower, is unlikely to be completely filled before lateral growth from the channel opening closes off the top of the channel. Hence, to avoid subsurface voids, aspect ratios (width/depth) of channels were typically limited to ≥1.

Figure 1c,i−iii shows typical in-lens and secondary electron FE-SEM images of all-diamond electrode structures produced using the above procedure, including (i) a triple individually addressable pBDD band electrode (band widths of 90, 64, and 460 μm); (ii) 1.02 mm diameter macrodisk electrode; and (iii) a ring disk pBDD electrode (1.02 mm diameter disk, ring with 1.10 mm inner diameter and 1.33 mm outer diameter). Also displayed in Figure 1c,iv is an optical image of a top contacted ring disk electrode where the black electrode structures are clearly visible. A typical tapping mode AFM image recorded at the boundary between insulating and conducting diamond is shown in the Supporting Information, Section 2, for two different pBDD band electrodes (of dimension 0.1 mm × 10 mm and 1 mm × 10 mm). A height line profile taken across the boundary reveals that the pBDD electrode was recessed by approximately 9 nm relative to the insulating region. A very

dx.doi.org/10.1021/ac501092y | Anal. Chem. XXXX, XXX, XXX−XXX

slight recess is expected as the hardness of the pBDD lattice is partially compromised by the presence of boron and so higher doped regions polish slightly faster.[19] This recess is minimal in size compared to those produced using alternative etch-based fabrication processes, which can be several hundreds of nm in size.[13,20] AFM topography scans recorded in either the pBDD or insulating only regions of the surface revealed similar surface roughness values (<2 nm) for both.

The polycrystalline nature of the pBDD is clearly visible in the FE-SEM images in Figure 1c, with grains varying in size typically in the range of 1−50 μm. The contrast differences in the FE-SEM, most evident in the conducting regions of the surface, are associated with the nonuniform uptake of boron into different crystal facets in the polycrystalline material.[21] Interestingly, at the interface between the pBDD and insulating diamond, the grains appear to be generally aligned in a direction perpendicular to the interface (Figure 1c). For clarity, grain orientation is further highlighted in the Supporting Information, Section 3. This orientation suggests that these pBDD grains grow laterally from the diamond grains of the side walls of the insulating recess, rather than vertically from grains at the bottom. For the smaller width band and ring structures, e.g., Figure 1c,i,iii, the grain structure indicates that the entire band is dominated by lateral side wall growth as opposed to the larger structures, such as the pBDD disk in Figure 1c,ii, which is composed of both lateral and vertical growth grains. Importantly, for structures grown in the regions where vertically growing pBDD meets lateral growth pBDD, in all bar one of the eighteen structures examined in this study, optical microscopy and FE-SEM revealed the absence of surface voids in the region of the overgrown pBDD. Furthermore, from lasered cross sections of all-diamond electrodes, e.g., as shown in Figure 2a and in the Supporting Information, Section 3, no subsurface voids were observed, indicating that the grains intergrow.

Electrical contact to the all-diamond electrodes was achieved in two ways. The first was a top contacting Ti/Au method (see Experimental Section) and required the additional machining of recessed structures to form both BDD contact pads (Figure 1b,i,ii) and BDD electrical contact wires (Figure 1b,vi). This approach was found suitable for electrode structures such as bands, where contact pads could be incorporated without compromising the geometry of the electrode, when employed in an electrochemical cell. However, in the case of other electrodes such as the individually addressable ring disk electrode schematically presented in Figure 1b,vi, the top contact approach results in the ring structure being partially compromised (unable to form a complete ring). Furthermore, the electrical contact wires may also contribute to the electrochemical current.

Four point probe electrical measurements made using Ti/Au contacts (n = 3) over the current range of ±1 mA at T = 25 °C revealed a linear current−voltage relationship (R^2 > 0.99) and an overall resistance, R_{total}, of 1.46 Ω for the Ti/Au contacts,

$$R_{total} = R_{BDD} + 2R_{contact} \quad (1)$$

where R_{BDD} is the intrinsic resistance of the pBDD (resistivity = 0.45 mΩ m;[22] hence, for the bar length and area dimensions employed, R_{BDD} = ∼0.88 Ω) and $R_{contact}$ is the contact resistance. $R_{contact}$ was determined to be 1.7 ± 0.12 mΩ cm^2 for the Ti/Au contacts.

A more attractive approach to top contacting, as illustrated in Figure 1b,v, is electrically back contacting which also means that the entire front face of the all-diamond electrode can be exposed to solution. It has previously been shown that laser micromachining insulating diamond produces a conductive material with electrical properties similar to graphite.[23] Back contacting was thus achieved by laser machining a blind hole just through to the rear side of the pBDD electrode, as shown pictorially in the FE-SEM image, Figure 2a.

During lasering, a plasma is formed at the lasered face; rapid expansion during heating causes most of the diamond to be ablated from the hole in the gaseous oxidized form, e.g., CO, CO_2. A small proportion is, however, left behind in the form of a black, conductive soot-like deposit, which forms the NDC-conducting diamond contact. Note, most of the material can be removed by aggressive acid cleaning if required, e.g., when preparing the structure for a pBDD overgrowth (see Experimental Section). Blind holes were machined by removal of successive ∼30 μm thick layers of insulating diamond using a cross hatching approach, where the direction of the hatch was rotated by 60° with each layer. Rotational cross hatching was employed to ensure an even cut during lasering. White light interferometry was periodically employed to monitor the depth of the machined hole and to ensure that the cut extended to the bottom of the pBDD-filled recess but did not penetrate through to the top-side of the electrode, as shown in Figure 2b. The use of optical grade diamond made location of the laser in the black pBDD regions on the transparent diamond face a facile process, as shown by the optical image in the inset to Figure 2a. Note, opaque mechanical-grade insulating diamond could still be used; however, alignment marks are required to accurately position the laser. To determine the resistance of the lasered surface contact, an experiment equivalent to that that described above for the Ti/Au contact was performed. $R_{contact}$ (n = 3) was determined to be 2.5 ± 1.3 mΩ cm^2. The low magnitude of $R_{contact}$ for both the Ti/Au and lasered NDC contacts implies negligible ohmic drop due to $R_{contact}$.

To form the final contact, the lasered back contact holes were filled with conducting Ag DAG, inserted Cu multicore wires, and a hard epoxy used to fix the wires in place. When back contacting structures containing multiple closely spaced electrodes, it is important to consider the size of the entrance hole and the separation of the electrodes. This is to ensure that overlapping entrance holes do not electrically connect two adjacent electrodes.

FE-SEM images of cross sectioned back contact holes revealed a tapered structure. For example, drilling 1 mm deep into insulating diamond with a 500 μm diameter entry hole resulted in a base diameter of ∼300 μm. This is most likely due to the sidewalls receiving a lower energy density due to the perpendicular orientation with respect to the beam direction and therefore machining less efficiently. The tapering of the back contact hole is clearly evident in the inset picture to Figure 2a, showing multiple band structures individually addressed. It is evident from this image that electrical shorting has not occurred during the contacting procedure.

BDD Characterization. The all-diamond electrodes where characterized by FE-SEM (as shown in Figure 1c), Raman spectroscopy, and electrochemistry, i.e., solvent windows, capacitance, and CV, the latter for the fast outer sphere one electron transfer redox species, $Ru(NH_3)_6^{3+/2+}$.[2] In total, n = 18 different electrodes were assessed, including ten band electrodes with width dimensions in the range of 50−1000 μm; the length was fixed at 10 mm; one dual band electrode (width dimensions of 60 and 460 μm); one triple band electrode

dx.doi.org/10.1021/ac501092y | Anal. Chem. XXXX, XXX, XXX−XXX

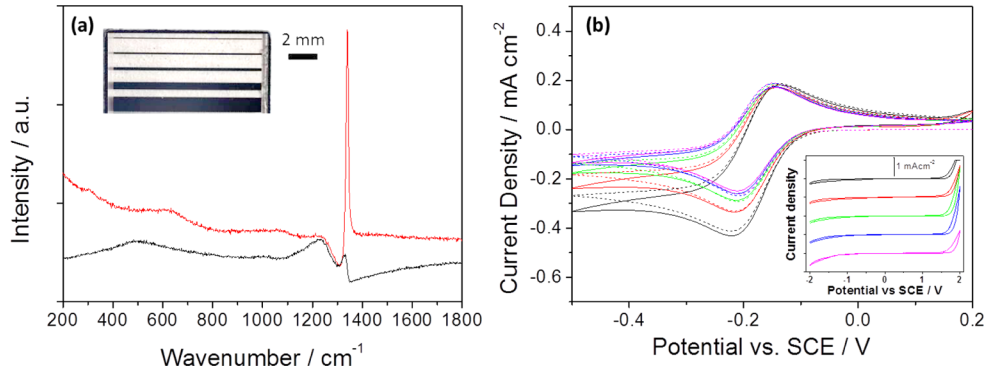

Figure 3. All-diamond individually addressable band electrodes (back contacted). Band lengths were all 10 mm, and widths were in the range of 50 μm to 1 mm. (a) Typical Raman spectra recorded from higher (black) and lower (red) doped grains on an electrode with width of 200 μm. The inset shows a photograph (image Copyright 2014 Jonathan C. Newland) of a ten band all diamond electrode device. (b) Experimental (solid lines) and simulated (dashed lines) CVs for 1 mM $Ru(NH_3)_6^{3+}$ reduction/oxidation recorded at 100 mV s^{-1}, in 0.1 M KNO_3, on different width pBDD band electrodes, 1 mm (black), 500 μm (red), 200 μm (green), 100 μm (blue), and 50 μm (magenta). Inset shows solvent windows recorded in 0.1 M KNO_3 at 100 mV s^{-1} for the same five electrodes (color scheme is the same).

(width dimensions of 64, 90, and 460 μm); one disk electrode of diameter 1.02 mm and two ring disk electrodes of the dimensions given in Figure 1c,iii and Figure SI2 (Supporting Information, Section 1). Of the 18 electrodes fabricated, only one was deemed unsuitable for further investigation due to an electrical contact failure; the NDC back contact had partially penetrated through to the front electrode face resulting in a significant increase in the measured capacitance and damage to the electrode surface.

Representative data is shown in Figure 3, for five individually addressable, NDC back-contacted pBDD band electrodes with widths of 50, 100, 200, 500, and 1000 μm (micro- to macroscale), shown optically in the inset to Figure 3a. Further characterization data is provided in the Supporting Information, Sections 1 and 5, for the ring and disk electrodes, respectively.

Micro-Raman spectroscopy (514.5 nm) is useful for ascertaining NDC and qualitatively assessing boron concentration;[24] however, the results must be treated with caution as micro-Raman will only sample a small area of the surface at any one time. Spot size depends on optical magnification, but typically, for 50×, the spot size is ~5 μm. Hence, either micro-Raman NDC mapping must be undertaken,[2] although this is a very lengthy procedure especially if the electrode is macro-sized, or the data must be used in combination with electrochemical analysis.

Figure 3a shows typical Raman spectra, recorded on both high (black line) and lower doped (red line) facets of the 200 μm wide band electrode, and is typical of those recorded on other bands and in other regions of the same electrode. The sp^3 peak, which is observed at 1332 cm^{-1} in undoped polycrystalline diamond, is clearly seen, although it has shifted slightly in peak position and decreased in peak intensity, due to the high boron concentration.[2] The asymmetry of the peak (Fano resonance) also reflects the high levels of boron in the lattice, where a Fano resonance is typically observed for boron dopant levels ~>10^{20} B atoms cm^{-3}, which decreases in symmetry the higher the average boron content. Peaks present at ~500 and ~1230 cm^{-1} are also indicative of the high doping levels. NDC is observed by the presence of broader peaks between 1400 and 1600 cm^{-1}[25] and would be more likely to occur in the higher doped regions.[2] We see no evidence of NDC in the Raman spectra recorded.

The most effective way of ascertaining NDC is to record CV solvent windows in background electrolyte. Electrochemical analysis samples the entire electrode area and in background electrolyte both capacitive and surface oxidation/reduction processes contribute to the observed CV response. In particular, nonfaradaic oxidation of NDC results in an appreciable current flow just before water oxidation. Furthermore, although dissolved oxygen cannot be electrocatalytically reduced on a BDD surface, oxygen is sluggishly reduced in the presence of NDC, resulting in an appreciable cathodic current in the negative window. CVs were recorded at 100 mV s^{-1} in 0.1 M KNO_3 and are shown for the five band electrodes in the inset to Figure 3b. Importantly, for all five electrodes, the window is featureless until water electrolysis takes place indicative of negligible NDC. For these electrodes, solvent windows in the range of 3.62−3.78 V were recorded (where the anodic and cathodic potential limits are defined as the potential at which a current of 0.4 mA cm^{-2} is passed for water electrolysis) comparing well with that recorded previously for pBDD grown under similar conditions.[2] The one electrode, which contained a surface void, showed a notable difference in solvent window characteristics, compared to the other electrodes, as shown in the Supporting Information, Section 4. Here, a solvent window of 2.45 V was recorded and clear features were present in the CV, which correlate with the presence of NDC.

Capacitance measurements (double layer) were also used to assess (i) the quality of the pBDD synthesized and (ii) the seal between the pBDD and insulating diamond (poor seals lead to increased capacitance). Note that an anomalously high capacitance reading could also indicate a poorly contacted electrode. For the five band electrodes, double layer capacitances, C_{dl}, were determined by cycling at 100 mV s^{-1} over the potential range of ±0.08 V. Since

$$Q = C_{dl}\nu$$

C_{dl} can be determined by measuring the charge, Q, at 0 V at a fixed scan rate, ν. C_{dl} values of 6.61 μF cm^{-2} (50 μm band), 7.28 μF cm^{-2} (100 μm band), 6.73 μF cm^{-2} (200 μm band), 7.70 μF cm^{-2} (500 μm band), and 5.26 μF cm^{-2} (1 mm band) were obtained in line with that expected for the boron dopant levels employed during growth.[2,21]

dx.doi.org/10.1021/ac501092y | Anal. Chem. XXXX, XXX, XXX−XXX

Finally, to assess the electrochemical characteristics of the all-diamond electrodes, CV was typically performed at 100 mV s^{-1} in a solution containing 1 mM $Ru(NH_3)_6^{3+}$ and 0.1 M KNO_3; more detailed studies involved varying the scan rate, typically in the range of 10−500 mV s^{-1} (as shown in the Supporting Information, Section 1, for an all-diamond ring electrode). Figure 3c shows the CV characteristics, recorded at 100 mV s^{-1} for the five band electrodes (solid lines) of different widths. COMSOL, as described in the Supporting Information, Section 1, was employed to simulate the expected CV response for each electrode (dotted line), assuming diffusion is rate limiting. The close agreement of the experimental and simulated data indicates that the pBDD electrodes are behaving as diffusion-limited "metal-like" electrodes, for their defined geometries. Also shown in the Supporting Information, Section 5, are characterization data for the all-diamond disk electrode.

CONCLUSIONS

Using a laser micromachining approach, where recessed structures can be machined into insulating diamond, then overgrown with pBDD, and finally polished (lapped) flat to reveal a coplanar structure, it is possible to fabricate individually addressable all-diamond electrodes of any geometry. This approach is demonstrated herein with the fabrication of individually addressable all-diamond disks, ring disk, and macro- and microband electrodes. We find that the smallest controllable electrode size is limited to ∼50 μm × 50 μm, taking into account the technical limit of the laser micromachiner, the aspect ratio of the recessed structure produced, and the ease at which pBDD can be grown into the recess, avoiding defects and NDC growth. The resolution of this fabrication methodology could be increased further by employing improved lithographic and processing techniques.

Low resistance electrical contacting is possible using either Ti/Au top contacts or NDC back contacts, the latter increasing the range of electrode geometries which can be processed and the usability of the resulting electrode, especially in harsh and aggressive environments for long periods of time. The all-diamond electrodes are shown to exhibit the same characteristics of highly doped, negligible NDC content, pBDD grown in bulk form, thus demonstrating that the quality and performance capabilities of the pBDD have not been compromised via growth into the recessed structures. Note that the use of optical grade insulating diamond also paves the wave for combined electrochemical spectroscopic measurements using the same device.

ASSOCIATED CONTENT

Supporting Information

(1) COMSOL simulation of CVs for fast electron transfer at different BDD electrode geometries; (2) AFM analysis of all-diamond electrodes; (3) FE-SEM images of all-diamond electrodes; (4) FE-SEM and solvent window characterization of a surface void; (5) electrochemical characterization of an all-diamond disk electrode. This material is available free of charge via the Internet at http://pubs.acs.org.

AUTHOR INFORMATION

Corresponding Author

*E-mail: j.macpherson@warwick.ac.uk.

Notes

The authors declare no competing financial interest.

ACKNOWLEDGMENTS

We thank Element Six for funding (M.B.J. and E.B.) and synthesis of the overgrown pBDD diamond electrodes. We acknowledge Advantage West Midlands and the European Regional Development Fund for providing some of the equipment used in this research.

REFERENCES

(1) (a) Swain, G. M.; Ramesham, R. *Anal. Chem.* **1993**, *65*, 345−351. (b) Panizza, M.; Cerisola, G. *Electrochim. Acta* **2005**, *51*, 191−199. (c) Martin, H. B.; Argoitia, A.; Landau, U.; Anderson, A. B.; Angus, J. C. *J. Electrochem. Soc.* **1996**, *143*, L133−L136.

(2) Hutton, L. A.; Iacobini, J. G.; Bitziou, E.; Channon, R. B.; Newton, M. E.; Macpherson, J. V. *Anal. Chem.* **2013**, *85*, 7230−7240.

(3) (a) Granger, M. C.; Witek, M.; Xu, J. S.; Wang, J.; Hupert, M.; Hanks, A.; Koppang, M. D.; Butler, J. E.; Lucazeau, G.; Mermoux, M.; Strojek, J. W.; Swain, G. M. *Anal. Chem.* **2000**, *72*, 3793−3804. (b) Yano, T.; Tryk, D. A.; Hashimoto, K.; Fujishima, A. *J. Electrochem. Soc.* **1998**, *145*, 1870−1876.

(4) Hutton, L.; Newton, M. E.; Unwin, P. R.; Macpherson, J. V. *Anal. Chem.* **2008**, *81*, 1023−1032.

(5) (a) Rao, T. N.; Yagi, I.; Miwa, T.; Tryk, D. A.; Fujishima, A. *Anal. Chem.* **1999**, *71*, 2506−2511. (b) Salimi, A.; Hyde, M. E.; Banks, C. E.; Compton, R. G. *Analyst* **2004**, *129*, 9.

(6) Prado, C. S.; Flechsig, G.-U.; Grundler, P.; Foord, J. S.; Marken, F.; Compton, R. G. *Analyst* **2002**, *127*, 329−332.

(7) Svorc, L.; Sochr, J.; Rievaj, M.; Tomčík, P.; Bustin, D. *Bioelectrochemistry* **2012**, *88*, 36−41.

(8) Wakerley, D.; Güell, A. G.; Hutton, L. A.; Miller, T. S.; Bard, A. J.; Macpherson, J. V. *Chem. Commun.* **2013**, *49*, 5657−5659.

(9) Hutton, L.; Newton, M. E.; Unwin, P. R.; Macpherson, J. V. *Anal. Chem.* **2009**, *81*, 1023−1032.

(10) Sarada, B. V.; Rao, T. N.; Tryk, D. A.; Fujishima, A. *J. Electrochem. Soc.* **1999**, *146*, 1469−1471.

(11) (a) Colley, A. L.; Williams, C. G.; Johansson, U. D.; Newton, M. E.; Unwin, P. R.; Wilson, N. R.; Macpherson, J. V. *Anal. Chem.* **2006**, *78*, 2539−2548. (b) Pagels, M.; Hall, C. E.; Lawrence, N. S.; Meredith, A.; Jones, T. G. J.; Godfried, H. P.; Pickles, C. S. J.; Wilman, J.; Banks, C. E.; Compton, R. G.; Jiang, L. *Anal. Chem.* **2005**, *77*, 3705−3708.

(12) Hutton, L. A.; Vidotti, M.; Iacobini, J. G.; Kelly, C.; Newton, M. E.; Unwin, P. R.; Macpherson, J. V. *Anal. Chem.* **2011**, *83*, 5804−5808.

(13) Hees, J.; Hoffmann, R.; Yang, N.; Nebel, C. E. *Chemistry* **2013**, *19*, 11287−11292.

(14) Wilson, N. R.; Clewes, S. L.; Newton, M. E.; Unwin, P. R.; Macpherson, J. V. *J. Phys. Chem. B* **2006**, *110*, 5639−5646.

(15) Balmer, R. S.; Brandon, J. R.; Clewes, S. L.; Dhillon, H. K.; Dodson, J. M.; Friel, I.; Inglis, P. N.; Madgwick, T. D.; Markham, M. L.; Mollart, T. P.; Perkins, N.; Scarsbrook, G. A.; Twitchen, D. J.; Whitehead, A. J.; Wilman, J. J.; Woollard, S. M. *J. Phys.: Condens. Matter* **2009**, *21*, 364221.

(16) Das, K.; Venkatesan, V.; Miyata, K.; Dreifus, D. L.; Glass, J. T. *Thin Solid Films* **1992**, *212*, 19−24.

(17) Knowles, M. Oxford Lasers, UK. Private communication, 2014.

(18) Butler, J. E.; Mankelevich, Y. A.; Cheesman, A.; Jie, M.; Ashfold, M. N. R. *J. Phys.: Condens. Matter* **2009**, *21*, 364201.

(19) Hird, J. R.; Field, J. E. *Proc. R. Soc. London A* **2004**, *460*, 3547−3568.

(20) (a) Smirnov, W.; Yang, N.; Hoffmann, R.; Hees, J.; Obloh, H.; Muller-Sebert, W.; Nebel, C. E. *Anal. Chem.* **2011**, *83*, 7438−7443. (b) Kiran, R.; Rousseau, L.; Lissorgues, G.; Scorsone, E.; Bongrain, A.; Yvert, B.; Picaud, S.; Mailley, P.; Bergonzo, P. *Sensors* **2012**, *12*, 7669−7681.

(21) Patten, H. V.; Meadows, K. E.; Hutton, L. A.; Iacobini, J. G.; Battistel, D.; McKelvey, K.; Colburn, A. W.; Newton, M. E.; Macpherson, J. V.; Unwin, P. R. *Angew. Chem., Int. Ed.* **2012**, *51*, 7002−7006.

(22) Diafilm EA: Enabling new electroanalytical applications. www.e6.com/sensors (accessed 31/01/2014).

(23) Alemanno, E.; Martino, M.; Caricato, A. P.; Corrado, M.; Pinto, C.; Spagnolo, S.; Chiodini, G.; Perrino, R.; Fiore, G. *Diamond Relat. Mater.* **2013**, *38*, 32−35.
(24) Fujishima, A.; Einaga, Y. A.; Rao, T. N.; Tryk, D. A. *Diamond Electrochemistry*; Elsevier: Boston, 2005.
(25) Prawer, S.; Nemanich, R. J. *Philos. Trans. R. Soc., A* **2004**, *362*, 2537−2565.

dx.doi.org/10.1021/ac501092y | *Anal. Chem.* XXXX, XXX, XXX−XXX